

## Self-assembled perovskite-spinel heterostructure on a highly distorted substrate

Y. M. Zhu, D. Ke, R. Yu, Y. H. Hsieh, H. J. Liu, P. P. Liu, Y. H. Chu, and Q. Zhan

Citation: [Applied Physics Letters](#) **102**, 111903 (2013); doi: 10.1063/1.4796037

View online: <http://dx.doi.org/10.1063/1.4796037>

View Table of Contents: <http://scitation.aip.org/content/aip/journal/apl/102/11?ver=pdfcov>

Published by the [AIP Publishing](#)

---

### Articles you may be interested in

[Localized Si enrichment in coherent self-assembled Ge islands grown by molecular beam epitaxy on \(001\)Si single crystal](#)

J. Appl. Phys. **113**, 033513 (2013); 10.1063/1.4775772

[Epitaxial self-assembly of multiferroic nanostructures](#)

J. Appl. Phys. **105**, 061615 (2009); 10.1063/1.3056160

[Phosphonate self-assembled monolayers on aluminum surfaces](#)

J. Chem. Phys. **124**, 174710 (2006); 10.1063/1.2186311

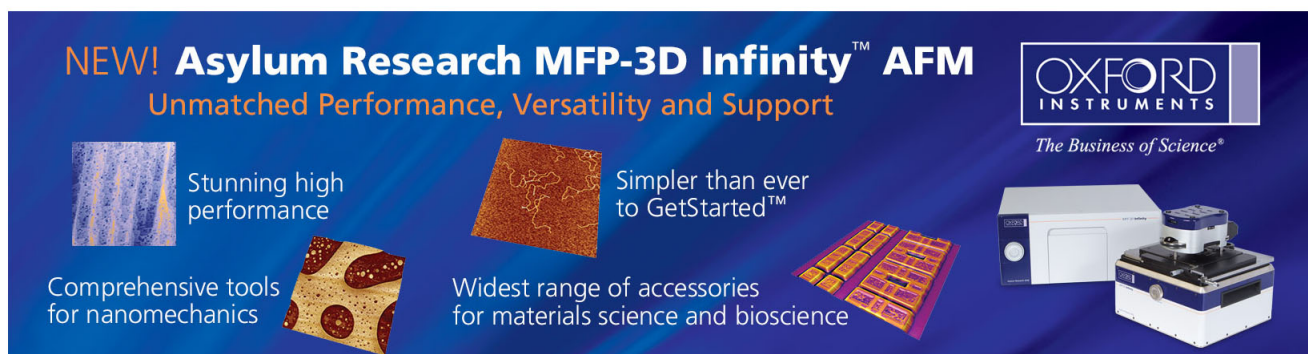
[Self-assembled CoAs nanostructures](#)

J. Vac. Sci. Technol. B **21**, 1760 (2003); 10.1116/1.1593649

[Self-assembly of epitaxial Ag nanoclusters on H-terminated Si\(111\) surfaces](#)

J. Appl. Phys. **94**, 743 (2003); 10.1063/1.1581341

---

The advertisement features a dark blue background with white and orange text. At the top left, it reads 'NEW! Asylum Research MFP-3D Infinity™ AFM' in large white letters, followed by 'Unmatched Performance, Versatility and Support' in orange. On the right, the Oxford Instruments logo is shown with the tagline 'The Business of Science®'. Below the text are four images: a blue textured surface, a brown textured surface, a grid of colorful squares, and the physical AFM instrument. Each image is accompanied by a short text description: 'Stunning high performance', 'Simpler than ever to GetStarted™', 'Comprehensive tools for nanomechanics', and 'Widest range of accessories for materials science and bioscience'.

## Self-assembled perovskite-spinel heterostructure on a highly distorted substrate

Y. M. Zhu,<sup>1</sup> D. Ke,<sup>1</sup> R. Yu,<sup>2</sup> Y. H. Hsieh,<sup>3</sup> H. J. Liu,<sup>3</sup> P. P. Liu,<sup>1</sup> Y. H. Chu,<sup>3</sup> and Q. Zhan<sup>1,a)</sup>

<sup>1</sup>Department of Material Physics and Chemistry, University of Science and Technology Beijing, Beijing 100083, China

<sup>2</sup>Department of Materials Science and Engineering, Beijing National Center for Electron Microscopy, Tsinghua University, Beijing 100084, China

<sup>3</sup>Department of Materials Science and Engineering, National Chiao Tung University, Hsinchu 30010, Taiwan

(Received 14 January 2013; accepted 6 March 2013; published online 18 March 2013)

The pattern configuration and interface structure in epitaxial BiFeO<sub>3</sub>-CoFe<sub>2</sub>O<sub>4</sub> heterostructures grown on (010)<sub>pc</sub> NdGaO<sub>3</sub> substrates have been investigated systematically by transmission electron microscopy and chemical analysis. The crystal orientation of CoFe<sub>2</sub>O<sub>4</sub> variants was tuned to [111]<sub>CFO</sub>, while BiFeO<sub>3</sub> kept [010]<sub>pc</sub> matching the substrate. Triangular prism-shaped CoFe<sub>2</sub>O<sub>4</sub> embedded in the BiFeO<sub>3</sub> matrix grew as an equilibrium island mode with {111}<sub>CFO</sub> as its surfaces and interfaces. Two types of BiFeO<sub>3</sub>-CoFe<sub>2</sub>O<sub>4</sub> orientation relationships were determined as (001)[010]<sub>BFO</sub>//(0-22)[111]<sub>CFO</sub> and (101)[010]<sub>BFO</sub>//(-220)[111]<sub>CFO</sub>. The results reveal that the dominant factors controlling the growth orientation of the present vertical heterostructures are surface energy anisotropy and atomic structure continuity. © 2013 American Institute of Physics. [<http://dx.doi.org/10.1063/1.4796037>]

Heterostructures provide a powerful route to manipulate the interplay of lattice, charge, orbital, and spin degrees of freedom in complex oxides, which covers a broad spectrum of intriguing functionalities and offers tremendous opportunities for next-generation electronic devices.<sup>1,2</sup> Among complex oxide heterostructures, high interface-to-volume ratio vertical nanostructures have drawn a considerable spotlight and been used to tune the functionalities. Examples can be found in the (La,Ca)MnO<sub>3</sub>-MgO system with tunable Curie temperatures,<sup>3</sup> the BaTiO<sub>3</sub>-CoFe<sub>2</sub>O<sub>4</sub> system with enhanced interfacial coupling,<sup>4,5</sup> magnetic-field-assisted electrically controllable magnetoelectric coupling in CoFe<sub>2</sub>O<sub>4</sub>-BiFeO<sub>3</sub> (CFO-BFO),<sup>6</sup> low magnetic-field driven colossal magnetoresistance in (La,Sr)MnO<sub>3</sub>-ZnO,<sup>7,8</sup> abnormal dielectric response in BiFeO<sub>3</sub>-Sm<sub>2</sub>O<sub>3</sub>,<sup>9</sup> and enhanced ferroelectricity in BaTiO<sub>3</sub>-Sm<sub>2</sub>O<sub>3</sub>.<sup>10</sup> In this type of the heterostructures, the lattice misorientation of the constituent materials plays a key role in determining the couplings between phases. The studies so far on vertical columnar heterostructures are focused on the constituent materials with the same crystallographic orientations: a simple cube-on-cube orientation relationship between the component phases and also the substrate, which is solely determined by the orientation of substrate.<sup>11-16</sup> On the other hand, however, such structures and phase orientation were unitary and the tuning ability of properties is limited. It is well known that the degree of coupling between the ordered parameters and hence the significance of nanostructures are considerably dependent on the nanostructure configurations including domain patterns and shapes as well as structures and properties of the interfaces.<sup>17</sup> Exploring various crystallographic orientation relationships in the composite films become extremely important.

Recently, by taking the CFO-BFO self-assembled nanostructure as a model system, an effective approach was

demonstrated to control the relative orientations of CFO and BFO by strain engineering of BFO thin films using substrates with different crystal structures and lattice parameters.<sup>18</sup> It was also shown the relevant physics with different relative crystal orientations. The plentiful combination forms of nanostructures and regulations on the crystallographic orientation of the constituent phases can provide more ways on tailoring degrees of freedom of complex oxide heterostructures. However, the interface structure and the underline growth mechanisms on these new orientation combinations are yet to be addressed, which is a prerequisite to understand the coupling mechanism among ferroelectricity, magnetism, and elasticity. In the present study, microstructure, phase constituent, and orientation relationship have been investigated systematically on BiFeO<sub>3</sub>-CoFe<sub>2</sub>O<sub>4</sub> nanocomposite thin films grown on a (010)<sub>pc</sub> NdGaO<sub>3</sub> (NGO) substrate (subscript pc represents pseudocubic). Special crystallography orientation relationships in the epitaxial model system other than the traditional cube-on-cube one reported before were investigated in detail. The hetero-interface structure at an atomic scale was studied by high resolution transmission electron microscopy (HRTEM), and the growth mechanism was also discussed.

The nanocomposite thin films of BiFeO<sub>3</sub>-CoFe<sub>2</sub>O<sub>4</sub> were grown on orthorhombic perovskite (010)<sub>pc</sub>-NdGaO<sub>3</sub> substrates using a composite target with molar ratio of 0.65BFO-0.35CFO by pulsed laser deposition at 700 °C in O<sub>2</sub> (200 mTorr). BFO is a rhombohedrally distorted perovskite structure with the lattice parameter  $a_{pc} = 3.96 \text{ \AA}$  ( $R3c$ , S.G. 161). It displays a large ferroelectric characteristic at room temperature.<sup>19</sup> CFO is ferromagnetic with a cubic  $Fd3m$  spinel structure, which the parameters are  $a = b = c = 8.396 \text{ \AA}$ , approximately double unit cell of BFO. While NGO used as the substrate in the present paper is a perovskite structure with an orthorhombic distortion. Its space group is  $Pbn2_1$  with the lattice parameter of

<sup>a)</sup>Electronic mail: qzhan@mater.ustb.edu.cn

$a_{pc} = 3.85 \text{ \AA}$ .<sup>20</sup> The following indexing and discussion on NGO and BFO were referred to the pseudocubic structure for simplicity. The composition and microstructure were characterized by X-ray diffraction, transmission electron microscopy (TEM), and scanning transmission electron microscopy (STEM) techniques. Cross-section as well as plan-view samples for TEM studies were prepared by standard ion milling techniques. TEM investigations were carried out using an FEI Tecnai F20 equipped with high-angle annular dark-field detector. The electronic diffraction patterns were acquired at a JEOL-2010 microscope operating at 200 kV.

The films were characterized by X-ray diffraction to explore the quality and epitaxial growth situation. Distinct peaks for BFO and CFO were observed in addition to reflections from the NGO substrate in Fig. 1(a). The results indicated that the film exhibited high degree of crystallinity, and the two constituent phases had a good epitaxial orientation with NGO substrate. The out-of-plane oriented crystallographic relationship is determined to be  $(111)_{CFO} // (010)_{pc}BFO // (010)_{pc}NGO$ .

Figures 1(b)–1(f) are Z-dependent contrast low magnification morphologies of the BFO-CFO nanostructure on  $(010)_{pc}$ -oriented NGO substrate from both plan-view and cross-section orientations and the corresponding electron

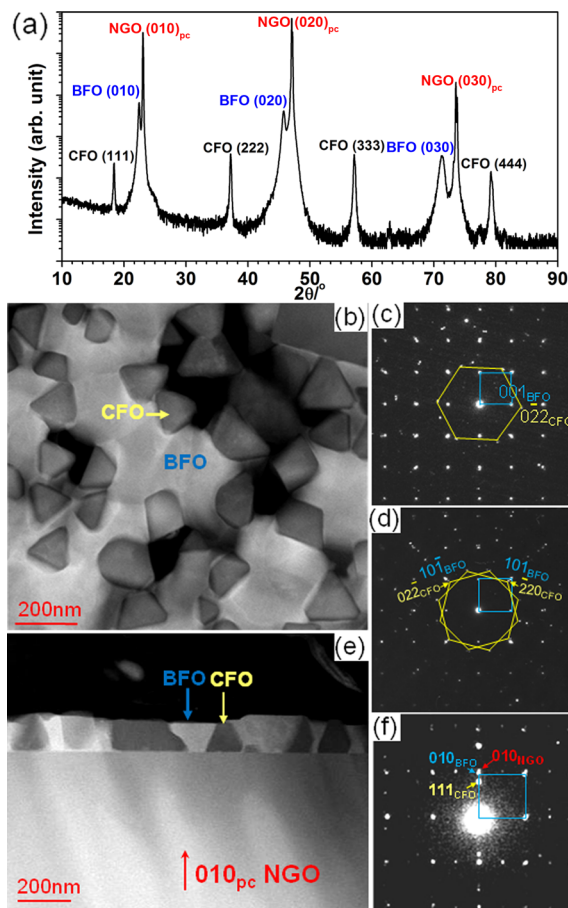


FIG. 1. (a) XRD  $\theta$ - $2\theta$  scan of  $\text{BiFeO}_3$ - $\text{CoFe}_2\text{O}_4$  composite films on  $(010)_{pc}$   $\text{NdGaO}_3$  substrate. (b) Low magnification Z-contrast image of the  $\text{BiFeO}_3$ - $\text{CoFe}_2\text{O}_4$  film in plan-view sample and the corresponding diffraction patterns with different in-plane orientation relationship (c) and (d). (e) High angle annular dark field (HAADF) image showing the cross-sectional morphology of the  $\text{BiFeO}_3$ - $\text{CoFe}_2\text{O}_4$  film. (f) Selected area diffraction pattern of the composite film and partial substrate in cross-sectional sample.

diffraction patterns (EDPs). Z-contrast imaging helps eliminate contrast contributions that originate from coherent strain effects and highlight mass-thickness differences. It is especially suitable for investigating phase separation in composite films when the atomic numbers “Z” of elements in two phases are adequately different. In our model system,  $\text{BiFeO}_3$  phase containing heavy atoms of Bi(83) exhibited much brighter contrast meanwhile  $\text{CoFe}_2\text{O}_4$  phase containing relative light Co(27) atoms presented darker contrast in strong atomic number Z-contrast images. Obviously, the two phases spontaneously separated and self-assembled during heteroepitaxial growth. On the  $(010)_{pc}$  NGO substrate, CFO nanopillars with no obvious shape anisotropy were embedded in the BFO matrix and extended through the whole film. The interfaces between the two constituent phases as well as the substrate were flat and sharp. The interface between BFO and CFO tilted about  $70^\circ$  to the substrate surface (Fig. 1(e)), which lay on  $\{111\}$  planes of CFO. It was confirmed by the following HRTEM image. The surface of CFO nanostructure presented a triangular-like platform with  $\{111\}_{CFO}$  planes as its surface while BFO exhibited a flat  $(010)_{pc}$  surface.

To understand the orientation relationship clearly, the selected area EDPs of the nanocomposite thin films were analyzed in detail. Two types of orientation relationships were obtained from plan-view EDPs, as shown in Figs. 1(c) and 1(d). Both of them revealed that  $[111]_{CFO}$  oriented variants of CFO coexisted in the nanocomposite film, with the triangular-like platforms rotating around  $[111]_{CFO}$  direction of CFO ( $[010]_{pc}$  BFO/NGO). Two types of typical orientation relationships between CFO and BFO can be determined as

$$(001)_{BFO} // (0-22)_{CFO}, [010]_{BFO} // [111]_{CFO} \text{ (Fig. 1(c))}$$

$$(101)_{BFO} // (-220)_{CFO}, [010]_{BFO} // [111]_{CFO} \text{ (Fig. 1(d))}$$

Also, the out of plane orientation relationship was obtained from the cross-sectional EDP (Fig. 1(f)):  $(111)_{CFO} // (010)_{BFO} // (010)_{NGO}$ , which is consistent with the XRD results. The existence of additional weak spots in the EDPs besides the main ones are probably due to the presence of some small crystal nucleus since the growth kinetic factors affect the nanostructures. Remarkably, the crystal orientation of triangular prism-shaped CFO nanopillars were tuned to  $[111]_{CFO}$  in the growth direction while BFO kept  $[010]_{pc}$  matching the NGO substrate. This interesting nanostructure configuration is quite different from previous reports of simple “cube-on-cube” orientation relationship between the two component phases and also the substrate studied extensively in perovskite-spinel systems.<sup>4,11–13</sup>

The normalized line profile of energy-dispersive X-ray spectroscopy (EDS) across a CFO nanopillar was collected to explore the composition distribution and chemical interaction across the interface of BFO and CFO, as shown in Fig. 2. The contents of Bi went down sharply from the BFO phase with a brighter contrast to the dark trapezoid shaped CFO phase while the tendency on the Co was reversed. Furthermore, the profile of Fe element in CFO revealed higher counts than those in BFO, which was consistent with the elemental stoichiometric ratio in each phase. The drastic change of the typical elements profiles at the interface demonstrated that the interdiffusion between BFO and CFO can

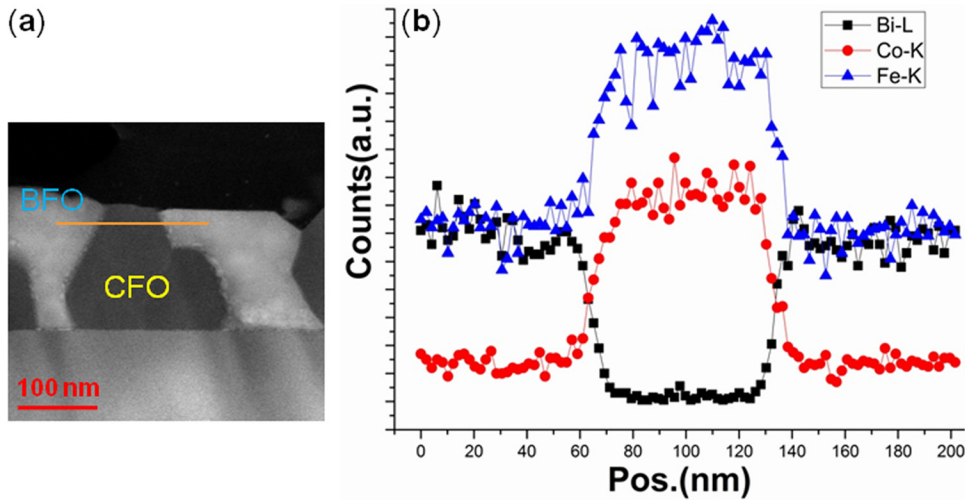


FIG. 2. (a) Cross-sectional HAADF images with a typical line for line scanning. (b) Line scan spectrum of basic elements obtained along the orange line marked in (a).

be negligible since perovskite and spinel have little solid solubility into each other. That is why the two phases can spontaneously separate and self-assemble during the heteroepitaxial growth.

The heterostructure with unusual combination patterns would exhibit intriguing interface structures. Figure 3 gives the HRTEM images of the BFO-CFO interface from plan-view and cross-sectional directions, respectively. Both of the HRTEM images revealed sharp and well-defined interfaces between BFO and CFO. The two phases exhibited good epitaxial relationships:  $(001)[010]_{\text{BFO}}// (0-22)[111]_{\text{CFO}}$  (Fig. 3(a)) and  $(111)[110]_{\text{CFO}}// (010)[100]_{\text{BFO}}$  (Fig. 3(c)), in accordance with one of the two typical orientation relationships revealed in Fig. 1(c). The interface between BFO and CFO was along  $[110]_{\text{CFO}}/[100]_{\text{BFO}}$  direction and lay on the  $\{111\}_{\text{CFO}}$  plane with  $70^\circ$  tilt to the  $(010)_{\text{pc}}$  substrate surface (Fig. 3(c)). In order to reveal the lattice mismatch, HRTEM

images were Fourier filtered by keeping only the Fourier component parallel to the interface, as shown in Figs. 3(b) and 3(d). The theoretical lattice mismatch of bulk BFO ( $hkl$ ) and CFO ( $h'k'l'$ ) planes can be calculated by the formula

$$\delta = \frac{|d_{(hkl)\text{BFO}} - d_{(h'k'l')\text{CFO}}|}{(d_{(hkl)\text{BFO}} + d_{(h'k'l')\text{CFO}})/2}. \quad (1)$$

Along the projection of  $[010]_{\text{BFO}}/[111]_{\text{CFO}}$  direction, the theoretical lattice mismatch between BFO(001) planes and CFO(0-22) planes is about  $\sim 30\%$ . It matches the misfit exhibited in Fig. 3(b), in which an extra plane of (0-22)CFO was observed around every three CFO planes. Meanwhile, along the  $[100]_{\text{BFO}}/[110]_{\text{CFO}}$  direction, the one dimensional Fourier filtered image (Fig. 3(d)) revealed that an extra (010) plane of BFO appeared about every five BFO planes, corresponding to a calculated lattice misfit of  $\sim 20\%$ . Thus, the lattice mismatch was almost relaxed both in the film plane and normal to the film. When modeling the physical properties of the composite thin films, the strain effect on the physical properties can be neglected safely, i.e., the ground-state properties (elasticity, ferroelectricity, and magnetism) of BFO and CFO can be used.

A high-resolution triple junction close to the NGO substrate is shown in Figure 4. The c-axis of orthorhombic NGO substrate lay in-plane confirmed by the periodic lattice of 0.77 nm, which is a typical character in an orthorhombic structure. Good wettability of BFO with the substrate was observed and  $(111)_{\text{CFO}}$  planes formed as the interfaces between the constituent phases and also with the substrate. It needs to emphasize that the CFO nanopillars rotated around  $[111]_{\text{CFO}}$  growth direction and presented a prism shape in the present study. Therefore, it is not easy to obtain a clear edge-on lattice image of CFO from the cross-sectional projection.

The plentiful combination forms of vertical nanostructures and regulations on the crystallographic orientation as well as the defined interface structures between the constituent phases may provide plentiful choices to tailor degrees of freedom. Thus, one can manipulate the functionalities in strong correlated complex oxides and offer attractive possibilities for device applications. In the present study, CFO

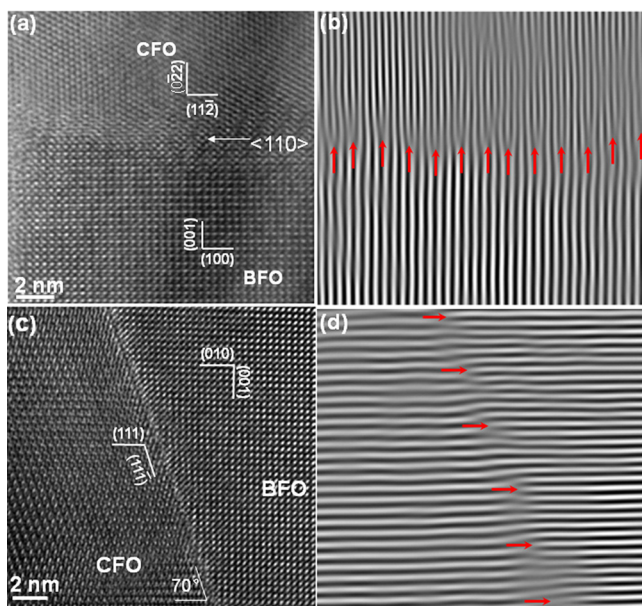


FIG. 3. (a) A high resolution TEM image in plan-view  $[010]_{\text{BFO}}/[111]_{\text{CFO}}$  direction showing the interface. (b) The one dimensional Fourier filtered image of (a). (c) High resolution cross-section TEM image of the  $\text{BiFeO}_3/\text{CoFe}_2\text{O}_4$  interface with the incident beam direction along  $[100]_{\text{BFO}}/[110]_{\text{CFO}}$ . (d) The corresponding one dimensional Fourier filtered image of (c), revealing the lattice mismatch of BFO(010) and CFO(111) planes.

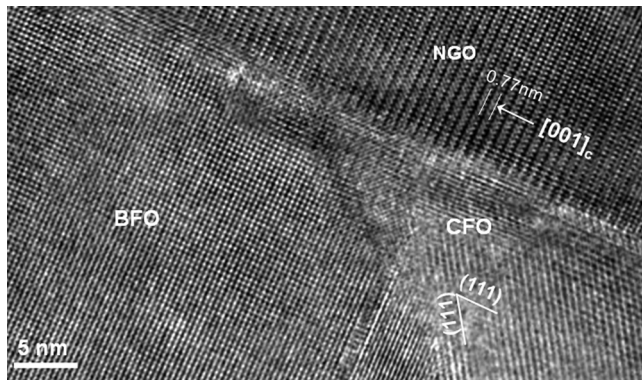


FIG. 4. A high resolution cross-sectional TEM image showing BFO-CFO-substrate triple junction in the NGO/BFO[100]<sub>c</sub> direction.

nanopillars on the NGO substrate with no obvious shape anisotropy resulted in quite different magnetic hysteresis loops both in-plane and out of plane directions, compared with that of CFO on Slater-type orbital (STO) with cube-on-cube orientations.<sup>18</sup> In fact, many thermodynamic factors may affect the pattern configurations of such vertical nanostructures during heteroepitaxial growth, such as the interfacial energy, surface energy, elastic energy, etc. And of course the difference of the crystal structure and atomic structural continuity between the constituent phases and perovskite substrates should be also taken into account. Figures 5(a) and 5(b) give the crystal structure model of cubic CFO and orthorhombic perovskite NGO, respectively. There is no distortion in the

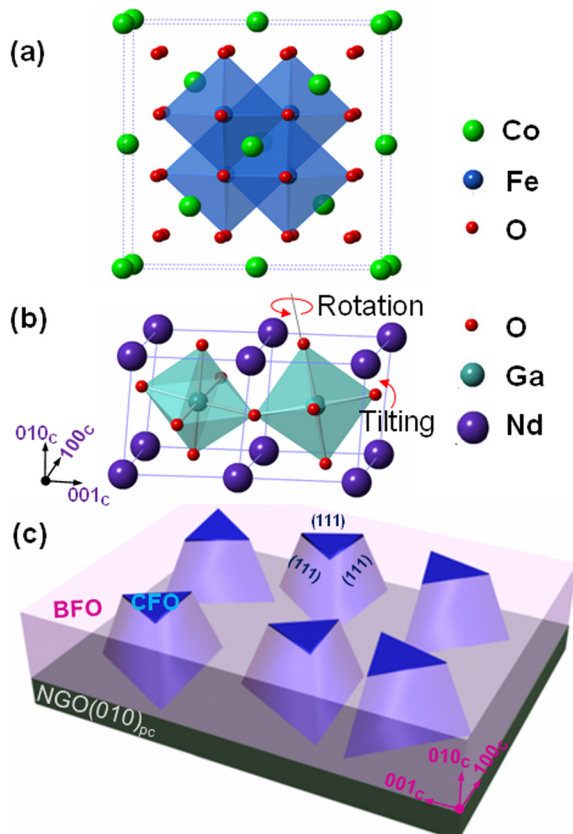


FIG. 5. (a) Unit cell of spinel CFO with cubic structure. (b) Unit cell of orthorhombic distorted NGO structure with the rotation and tilting of  $\text{GaO}_6$  octahedra. (c) Three-dimensional model for CFO-BFO films grown on  $(010)_{pc}$  NGO substrate.

spinel structure of CFO while NGO has an orthorhombic distorted perovskite structure with the pseudo-cubic lattice parameter of  $a_{pc} \approx 3.85 \text{ \AA}$ . It is worth to note that the lattice mismatch between CFO and NGO is relative larger, around 9%. The most important thing is that the  $\text{GaO}_6$  octahedra in NGO distorts heavily, which rotates about  $10.52^\circ$  around  $[001]_{pc}$  c-axis and tilts  $\sim 13.44^\circ$  in an opposite direction (determined using the measurement method proposed by Zayak *et al.*<sup>21</sup>). The distortion degree of NGO is much larger compared with those used in most cases before, such as the ideal cubic  $\text{SrTiO}_3$  or rhombohedral  $\text{LaAlO}_3$  perovskite substrates on which the vertical nanostructures exhibit cube-on-cube relations with the substrates.<sup>13,15,17,22</sup> Thus the lattice matching and atomic structural continuity decrease a lot when CFO phase with a spinel structure is grown on a heavily distorted NGO perovskite substrate. Therefore, the constraint effect of the NGO substrate on the growth orientation of CFO is weakened, and the surface energy anisotropy of CFO controls its growth orientation. On a  $(010)_{pc}$  orientated NGO substrate, CFO prefers to grow in an equilibrium island mode with  $\{111\}_{CFO}$  as its surfaces and interfaces since its  $\{111\}$  planes have the lowest surface energy.<sup>23</sup> Therefore, CFO formed the triangular prism-shaped islands with  $\{111\}_{CFO}$  as its surfaces and interfaces. For BFO with a perovskite structure, the  $\{100\}$  planes typically have the lowest surface energy. When grown on a  $(010)_{pc}$  orientated NGO substrate, BFO wets the substrate surface and keeps  $[010]$  orientation during the epitaxial growth since both of them have a perovskite structure. The schematic of an ideal structure model for BFO-CFO films on a  $(010)_{pc}$  NGO substrate is shown in Fig. 5(c).

In principle, the complicated strain state in the films should also be considered, which was emphasized a lot previously. Orthorhombic NGO applies an in-plane anisotropic compressive stress to both BFO and CFO. It is known that the crystal structure of BFO is sensitive to the applied stress, which may affect the growth mode of CFO in turn. However, according to our results shown in Fig. 3, the misfit strain between BFO and CFO was almost released. In practice, no obvious shape anisotropy on CFO nanopillars was observed. CFO nanopillars rotated around  $[111]_{CFO}$  direction in the  $(111)_{CFO}$  plane and variants formed instead. Therefore, the anisotropic strain is not a dominant factor affecting the formation of CFO in the present BFO-CFO/NGO system, confirming the importance of the surface energy anisotropy and the atomic structure continuity on tuning the configuration of vertical nanostructures.

In conclusion, our results demonstrate an attractive nanostructure configuration with unusual heterointerface structures and orientation relationships in the  $\text{BiFeO}_3\text{-CoFe}_2\text{O}_4$  model system when grown on  $[010]_{pc}$   $\text{NdGaO}_3$  substrates. CFO nanopillars with no obvious shape anisotropy were distributed homogeneously in the BFO matrix. The crystal orientation of CFO nanopillars was tuned to  $[111]_{CFO}$  in the growth direction, while BFO kept  $[010]_{pc}$  matching the NGO substrate. Triangular prism-shaped CFO rotated around the  $[111]_{CFO}$  growth direction in the  $(111)_{CFO}/(010)_{BFO/NGO}$  plane and grew in an equilibrium island mode with  $\{111\}_{CFO}$  as its surfaces and interfaces. The analysis shows that the dominant factors controlling the

growth orientation of the present vertical nanostructures are surface energy anisotropy and atomic structure continuity.

This work was supported by the National Natural Science Foundation of China with Grant Nos. 50971015, 50931003, and 51071092, and also the program of National Basic Research Development Plan with Grant 2011GB108002. The work in National Chiao Tung University was supported by the National Science Council, R.O.C. (NSC-101-2119-M-009-003-MY2), Ministry of Education, R.O.C. (MOE-ATU 101W961), and Center for interdisciplinary science of National Chiao Tung University.

- <sup>1</sup>S. M. Wu, S. A. Cybart, P. Yu, M. D. Rossell, J. X. Zhang, R. Ramesh, and R. C. Dynes, *Nature Mater.* **9**(9), 756 (2010).
- <sup>2</sup>L. W. Martin and R. Ramesh, *Acta Mater.* **60**(6–7), 2449 (2012).
- <sup>3</sup>V. Moshnyaga, B. Damaschke, O. Shapoval, A. Belenchuk, J. Faupel, O. I. Lebedev, J. Verbeeck, G. van Tendeloo, M. Mucksch, V. Tsurkan, R. Tidecks, and K. Samwer, *Nature Mater.* **2**(4), 247 (2003).
- <sup>4</sup>H. Zheng, J. Wang, S. E. Lofland, Z. Ma, L. Mohaddes-Ardabili, T. Zhao, L. Salamanca-Riba, S. R. Shinde, S. B. Ogale, F. Bai, D. Viehland, Y. Jia, D. G. Schlom, M. Wuttig, A. Roytburd, and R. Ramesh, *Science* **303**(30), 661 (2004).
- <sup>5</sup>H. Zheng, J. Wang, L. Mohaddes-Ardabili, M. Wuttig, L. Salamanca-Riba, D. G. Schlom, and R. Ramesh, *Appl. Phys. Lett.* **85**(11), 2035 (2004).
- <sup>6</sup>F. Zavaliche, H. Zheng, L. Mohaddes-Ardabili, S. Y. Yang, Q. Zhan, P. Shafer, E. Reilly, R. Chopdekar, Y. Jia, and P. Wright, *Nano Lett.* **5**(9), 1793 (2005).
- <sup>7</sup>J. L. MacManus-Driscoll, P. Zerrer, H. Wang, H. Yang, J. Yoon, A. Fouchet, R. Yu, M. G. Blamire, and Q. Jia, *Nature Mater.* **7**(4), 314 (2008).

- <sup>8</sup>A. Chen, Z. Bi, C. F. Tsai, J. H. Lee, Q. Su, X. Zhang, Q. Jia, J. L. MacManus Driscoll, and H. Wang, *Adv. Funct. Mater.* **21**(13), 2423 (2011).
- <sup>9</sup>H. Yang, H. Wang, J. Yoon, Y. Wang, M. Jain, D. M. Feldmann, P. C. Dowden, J. L. MacManus Driscoll, and Q. Jia, *Adv. Mater.* **21**(37), 3794 (2009).
- <sup>10</sup>S. A. Harrington, J. Zhai, S. Denev, V. Gopalan, H. Wang, Z. Bi, S. A. T. Redfern, S. H. Baek, C. W. Bark, and C. B. Eom, *Nat. Nanotechnol.* **6**(8), 491 (2011).
- <sup>11</sup>Z. Tan, J. Slutsker, and A. L. Roytburd, *J. Appl. Phys.* **105**(6), 061615 (2009).
- <sup>12</sup>H. Zheng, F. Straub, Q. Zhan, P. L. Yang, W. K. Hsieh, F. Zavaliche, Y. H. Chu, U. Dahmen, and R. Ramesh, *Adv. Mater.* **18**(20), 2747 (2006).
- <sup>13</sup>I. Levin, J. Li, J. Slutsker, and A. L. Roytburd, *Adv. Mater.* **18**(15), 2044 (2006).
- <sup>14</sup>J. Li, I. Levin, J. Slutsker, V. Provenzano, P. K. Schenck, R. Ramesh, J. Ouyang, and A. L. Roytburd, *Appl. Phys. Lett.* **87**(7), 072909 (2005).
- <sup>15</sup>N. Dix, R. Muralidharan, J. Guyonnet, B. Warot-Fonrose, M. Varela, P. Paruch, F. Saánchez, and J. Fontcuberta, *Appl. Phys. Lett.* **95**(6), 062907 (2009).
- <sup>16</sup>Q. Zhan, R. Yu, S. P. Crane, H. Zheng, C. Kisielowski, and R. Ramesh, *Appl. Phys. Lett.* **89**(17), 172902 (2006).
- <sup>17</sup>H. Zheng, Q. Zhan, F. Zavaliche, M. Sherburne, F. Straub, M. P. Cruz, L. Q. Chen, U. Dahmen, and R. Ramesh, *Nano Lett.* **6**(7), 1401 (2006).
- <sup>18</sup>S.-C. Liao, P.-Y. Tsai, C.-W. Liang, H.-J. Liu, J.-C. Yang, S.-J. Lin, C.-H. Lai, and Y.-H. Chu, *ACS Nano* **5**(5), 4118 (2011).
- <sup>19</sup>I. Sosnowska, R. Przeniosło, P. Fischer, and V. A. Murashov, *J. Magn. Magn. Mater.* **160**, 384 (1996).
- <sup>20</sup>L. Vasylechko, M. Berkowski, A. Matkovskii, W. Piekarczyk, and D. Savvitskii, *J. Alloy. Compd.* **300**, 471 (2000).
- <sup>21</sup>A. T. Zayak, X. Huang, J. B. Neaton, and K. M. Rabe, *Phys. Rev. B* **74**(9), 094104 (2006).
- <sup>22</sup>N. Dix, R. Muralidharan, J.-M. Rebled, S. Estradeá, F. Peiroá, M. Varela, J. Fontcuberta, and F. Saánchez, *ACS Nano* **4**(8), 4955 (2010).
- <sup>23</sup>R. K. Mishra and G. Thomas, *J. Appl. Phys.* **48**(11), 4576 (1977).